Published August 8, 2019

Original Research

Core Ideas

- Water retention and spectral induced polarization were measured for biochar in sand.
- Water retention curves could be fitted by using a dual porosity model.
- Residual water content was found to increase with the addition of biochar.
- The polarization of sand–biochar mixtures was much larger than that for sand.
- Spectral induced polarization may be suitable for monitoring biochar in the field.

Spectral Induced Polarization of Biochar in Variably Saturated Soil

Z. Gao, F.-H. Haegel,* O. Esser, E. Zimmermann, H. Vereecken, and J.A. Huisman

Biochar is considered a promising soil amendment, but an effective method to detect and characterize the spatial distribution and temporal dynamics of biochar in soil is still missing. The aim of this study is to investigate the ability of the spectral induced polarization (SIP) method for the noninvasive detection of biochar in unsaturated sandy media. In particular, a pure sand and two sand–biochar mixtures with 1 and 2% biochar made from pine (*Pinus* spp.) wood by pyrolysis at 800°C were investigated. The measured SIP spectra as a function of saturation were interpreted by fitting a Cole–Cole model to the low-frequency part of the SIP measurements. The porous nature of the biochar particles strongly affected the SIP response of the partially saturated sand–biochar mixtures. Due to the high residual water content of the biochar in a dry background, the relationship between bulk electrical conductivity and water saturation was nonlinear in a log–log representation. This nonlinear behavior could adequately be explained with a dielectric mixing model that considered the drainage of the biochar particles. Both the measured phase and chargeability of the sand–biochar mixtures showed a complex dependence on water saturation. This was attributed to the decrease in polarization strength of the biochar particles with desaturation and the simultaneous increase in phase of the sand background. Overall, the results of this study suggest that field SIP measurements may be a promising tool for the characterization and monitoring of biochar amendments to agricultural soils.

Abbreviations: DC, direct current; EDL, electrical double layer; MSO, multistep outflow; PMMA, poly(methyl methacrylate); PW800, biochar made by pyrolysis at 800°C from pine wood; SIP, spectral induced polarization.

Z. Gao, F.-H. Haegel (ORCID iD 0000-0002-2189-1792), O. Esser, H. Vereecken (ORCID iD 0000-0002-8051-8517), and J.A. Huisman (ORCID iD 0000-0002-1327-0945), Institute of Bio- and Geosciences–Agrosphere (IBG-3), Forschungszentrum Jülich, D-52425 Jülich, Germany; E. Zimmerman (ORCID iD 0000-0003-1517-6597), Central Institute of Engineering, Electronics and Analytics–Electronic Systems (ZEA-2), Forschungszentrum Jülich, D-52425 Jülich, Germany. *Corresponding author (f.h.haegel@fz-juelich.de).

Received 18 Dec. 2018.
Accepted 31 May 2019.

Citation: Gao, Z., F.-H. Haegel, O. Esser, E. Zimmermann, H. Vereecken, and J.A. Huisman. 2019. Spectral induced polarization of biochar in variably saturated soil. Vadose Zone J. 18:180213. doi:10.2136/vzj2018.12.0213

Biochar is obtained from biomaterials by carbonization at elevated temperature using different types of processes, among which the most important are pyrolysis (with exclusion of oxygen), gasification (with oxygen deficiency), and hydrothermal carbonization (in contact with water under pressure). It exhibits a variety of tunable properties concerning structure, composition, surface chemistry, and stability, depending on the chosen process parameters (Cha et al., 2016; Weber and Quicker, 2018). Besides a range of other applications, biochar is considered to be a promising soil amendment. It has attracted considerable research interest in the last decade due to its potential for improving the water retention and nutrient availability of soils (Amoakwah et al., 2017; Arthur and Ahmed, 2017; Bikbulatova et al., 2018; Głąb et al., 2016). As a consequence of these ameliorating properties, biochar amendments can have a positive effect on crop yield, especially on marginal soils (Agegnehu et al., 2017). However, the long-term stability of biochar in soil and possible positive and negative environmental effects of biochar application are still being discussed (Kavitha et al., 2018; Kuppusamy et al., 2016; Mukherjee and Lal, 2014). An increasing amount of field trials with biochar as soil amendment have been initiated (Agegnehu et al., 2017), but an effective method to detect and characterize the spatial distribution and temporal dynamics of biochar in soil is still missing. Due to the inert nature of black carbon materials, it is far from straightforward to use classical chemical methods to separate and analyze biochar after it has been applied to the soil. For the same reason, the monitoring of long-term field experiments remains challenging with such methods.

Spectral induced polarization (SIP) has recently been proposed as a promising method to investigate biochar in soil (Gao et al., 2017) due to its noninvasive nature and its sensitivity to textural, geochemical, and hydrological properties of soil (Kemna et al., 2012). Spectral induced polarization measures the frequency-dependent complex electrical conductivity of soil in the millihertz to kilohertz frequency range. The real part of the electrical conductivity is attributed to the electromigration of charge carriers in the porous media, whereas the imaginary part of the electrical conductivity is determined by the transient storage of charge in the porous media (i.e., polarization processes) (Binley et al., 2005; Grunat et al., 2013; Ulrich and Slater, 2004). In the absence of conductive or semiconductive particles, the complex electrical conductivity is determined by ionic movement in the pore space and polarization processes in the electrical double layer (EDL) at the interface between the soil matrix and the pore fluid (Leroy et al., 2008). When conductive or semiconductive particles are present, additional polarization associated with electronic charge carriers within the particles occurs (Revil et al., 2015b; Wong, 1979). Due to the high mobility of these electronic charge carriers, an external electrical field leads to the fast buildup of a strong dipole moment in the conductive or semiconductive particles and the successive formation of an associated EDL in the surrounding electrolyte (Bücker et al., 2018). Since the mechanism of polarization is the same for conductive and semiconductive particles, both types of particles will be denoted as conductive below. The resulting polarization associated with conductive particles can be much stronger than usual EDL polarization (Hupfer et al., 2016; Weller et al., 2010).

Gao et al. (2017) presented first SIP measurements on saturated sand–biochar mixtures with four types of biochar. The results showed that two of these biochars exhibited strong polarization, which was attributed to the electrical conductivity of the biochar particles caused by the higher graphitization. Although the work of Gao et al. (2017) was a first promising step, it was focused on the SIP signature of biochar in saturated soil. For future field studies, it is also important to understand how unsaturated soil conditions affect the SIP signature of biochar in soil.

It is well established that saturation has a strong impact on the complex electrical conductivity of soils (Binley et al., 2005; Breede et al., 2012; Ghorbani et al., 2008; Grunat et al., 2013; Maineult et al., 2018; Ulrich and Slater, 2004). Mechanistic explanations of how saturation affects the SIP signal have invoked changes in the effective excess charge associated with the EDL around a soil particle (Jougnot et al., 2010) or the change of an effective length-scale of the ion-selective pore throats in the porous media (Titov et al., 2002, 2004). Recently, Maineult et al. (2018) simulated the frequency-dependent complex electrical conductivity for drainage and imbibition of pore networks and found that key features of the available experimental data for unsaturated soils were well reproduced. To the best of our knowledge, there have been no studies yet that have investigated how saturation affects the polarization of conductive particles distributed within porous media. Within this context, the objective of this study is to investigate how the SIP spectra of sand–biochar mixtures change with saturation. For this purpose, three sand samples with 0, 1, and 2% additions of biochar (by weight) were drained by pressure, and SIP measurements were made at different saturation levels. A Cole–Cole model (Cole and Cole, 1941) was fitted to the SIP measurements, and the resulting dependence of the direct current (DC) electrical conductivity, the total chargeability, and the peak relaxation time on saturation are discussed within the context of previous findings and available mechanistic models for SIP.

Materials and Methods

Measurement Setup

The measurement setup developed by Breede et al. (2011) for joint SIP and hydraulic measurements was used in this study. This setup combined a multistep outflow (MSO) unit to drain the sample, and the electrical impedance spectrometer developed by Zimmermann et al. (2008) for SIP measurements (Fig. 1). The sample holder consisted of three connected cylindrical units made of poly(methyl methacrylate) (PMMA) with an inner diameter of 80 mm. The sample material was contained in the middle cell with 100-mm height and held in position by two ceramic plates at the top and bottom of the sample material. Above and below this middle unit, there were water-filled units to increase the SIP

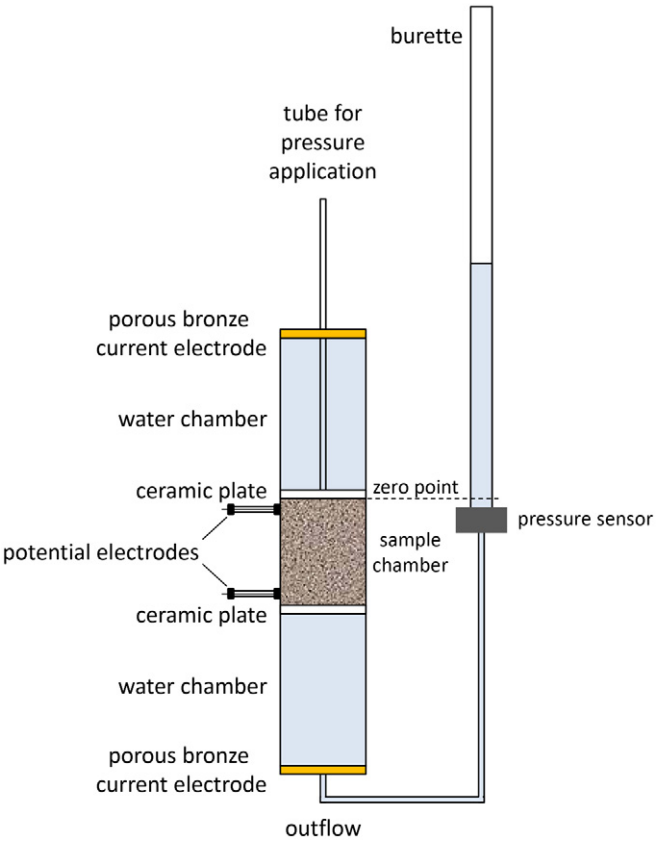

Fig. 1. Schematic drawing of the experimental setup for joint hydraulic and spectral induced polarization (SIP) measurements (after Breede et al., 2011).

measurement accuracy by increasing the distance between the current and potential electrodes (Zimmermann et al., 2008). To drain the sample material, air pressure was applied to the top ceramic plate by means of a tube. The drained water flowed into a burette, where the water height was measured by a pressure sensor and converted to the amount of drained water. If the dry weight of the solid phase at the start or the end of the experiment is known, the amount of drained water can be used to calculate the volumetric water content of the sample at any time.

A four-point electrode array was used to make SIP measurements in the millihertz to kilohertz frequency range. Porous bronze plate electrodes at the top and bottom of the sample holder were used to inject current (see Fig. 1). Potentials were measured using two custom-made nonpolarizable electrodes consisting of a small tube of PMMA with a diameter of 5 mm and a length of 210 mm with a 1-mm silver wire inside. One end of these electrodes consisted of a cone-shaped porous ceramic with a high air-entry pressure, which ensures reasonable electrical contact with the sample material even for unsaturated conditions. For more details and design considerations, the reader is referred to Breede et al. (2011).

Sample Preparation and Drainage Experiment

The complex conductivity of pure sand and two sand–biochar mixtures with 1 and 2% mass fractions of biochar was investigated as a function of saturation. The biochar was derived from pine wood chips through a pyrolytic process at 800°C. A sieved fraction of this biochar with a particle size between 1 and 2 mm was used to prepare the sand–biochar mixtures. The biochar particles have a skeletal density of ~1.80 g cm^{-3} determined using a pycnometer (AccuPyc 1330, Micromeritics) and a Brunauer–Emmett–Teller (BET) specific surface area of 181 m^2 g^{-1} determined by nitrogen adsorption (AUTOSORB-1, Quantachrome Instruments). Commercial sand (F36, Quarzwerke Frechen) with a particle diameter ranging from 0.125 to 0.250 mm and a mean particle diameter of 0.16 mm was used in this study. The grain density of the sand was 2.65 g cm^{-3}. The SIP measurements on saturated sand–biochar mixtures using this type of biochar have been presented in previous work (PW800 [biochar made by pyrolysis at 800°C from pine wood] in Gao et al., 2017). The saturated sand–biochar mixtures with 2% PW800 showed a relatively strong phase of more than 50 mrad owing to the relatively large pore surface and the presumed noticeable electrical conductivity of the particles expected from the low hydrogen/carbon ratio of this biochar. The total normalized chargeability of 0.007 S m^{-1} for an electrolyte conductivity of 0.1 S m^{-1} was comparable with the magnitude expected for conductive materials (Weller et al., 2010).

The preparation of the saturated sand–biochar mixtures proceeded as follows. First, biochar was immersed in a NaCl electrolyte with an electrical conductivity of 0.0450 S m^{-1} for 24 h before sample preparation to fully saturate the inner pores of the biochar particles and to avoid the biochar floating during sample preparation. The sand was moistened to a pasty consistence by adding the same NaCl electrolyte and stirring with a spoon. It was then fully mixed with the wet biochar until the biochar particles were well distributed in the sand. Next, the sample material was filled into the measurement cell with a similar wet packing procedure as used by Breede et al. (2011). The material was filled into the sample holder step by step while a layer of NaCl electrolyte was maintained above the sample material. Gentle stirring with a spoon removed air bubbles and avoided zonation leading to a visually homogeneous distribution of the biochar particles. After packing, the resulting porosity (ϕ) was calculated from the volume of the sample holder (V_{tot}), the masses of sand (w_s), and biochar (w_{bio}), the skeletal density of biochar (ρ_{bio}), and the grain density of sand (ρ_s) with

$$V_{tot} = \frac{w_s/\rho_s + w_{bio}/\rho_{bio}}{1-\phi} = (1-\upsilon)V_{tot} + \upsilon V_{tot} = \frac{w_s}{\rho_s(1-\phi_s)} + \frac{w_{bio}}{\rho_{bio}(1-\phi_{bio})} \quad [1]$$

The porosity of the pure sand sample ($\phi = \phi_s$) was 0.40, the porosity of the mixture with 1% biochar was 0.42, and the porosity of the mixture with 2% biochar was 0.44. If it is assumed that this increase in porosity is solely due to the addition of biochar, the equation can be split into individual additive volumes of sand and biochar with the volume fraction of biochar (υ) and the individual porosities of biochar (ϕ_{bio}) and sand (ϕ_s). The porosity of the biochar particles was estimated to be ~0.83 and the volume fractions of the 1 and 2% sand–biochar mixtures were estimated to be 6 and 10%, respectively.

After installation of the sample holder in the joint MSO-SIP setup, SIP measurements were made on the saturated sample. The complex impedance of the sample was measured at 97 frequencies approximately equally spaced between 1 mHz and 45 kHz in log-space. During each of the SIP measurements, alternating sinusoidal currents were injected starting from the maximum frequency, decreasing to the minimum frequency, and then returning back to the maximum frequency. These repeated measurements were used to check for drift in the SIP measurements (e.g., due to temperature variations, water outflow, or ion release from the solids during the 2.5-h-long SIP measurements). In all cases, it was found that this drift was negligible, and only the downward branch of the SIP measurements is presented in the remainder of this study. The three samples were drained in a series of pressure steps. The size of the pressure steps were chosen such that the decrease of saturation between two successive SIP measurements was small. When the outflow was negligible after the application of a pressure step, SIP measurements were made on consecutive days to verify that the sample was in approximate equilibrium. If the difference between the two consecutive SIP measurements was <2%, the next pressure step was applied. Using this procedure, the entire drainage experiment lasted for ~2 mo for each sample. The applied pressure was converted into suction at the bottom of the soil column (matric potential in centimeters). An overview of the applied suctions for the three samples is provided in Table 1. All measurements were performed

at a temperature of 20.0 ± 1.5°C with a temperature variation of <0.5°C during each SIP measurement.

The water content of the samples as a function of pressure head (h) obtained from the stepwise drainage of the three samples was fitted with the van Genuchten model for the water retention curve (van Genuchten, 1980):

$$\frac{\theta(h)-\theta_r}{\theta_s-\theta_r}=\left(1+|\alpha h|^n\right)^{-m} \quad [2]$$

where θ_r and θ_s are the residual and saturated soil water content, respectively, α is the inverse of the air-entry value, n is a shape factor related to the pore size distribution, and $m = 1 - 1/n$. In the case of the sand–biochar mixtures, the water content is described using a simple dual-porosity model with two domains (Šimůnek et al., 2003):

$$\theta(h)=\nu\theta_{bio}(h)+(1-\nu)\theta_{sand}(h) \quad [3]$$

where $\theta_{sand}(h)$ and $\theta_{bio}(h)$ are the water retention curves of the sand and the biochar.

Table 1. Applied suction steps ($|h|$) and the corresponding saturation values (S_w) for the pure sand and the two sand–biochar mixtures.

Sand		Sand–biochar mixture (1%)		Sand-biochar mixture (2%)	
$\|h\|$	S_w	$\|h\|$	S_w	$\|h\|$	S_w
cm	%	cm	%	cm	%
15	100	20	100	20	100
53	100	41	100	41	100
57	99	49	98	49	98
59	97	51	97	51	98
61	88	53	96	53	95
64	71	56	87	56	87
67	64	58	85	58	78
69	51	60	81	60	77
71	41	62	77	62	73
74	35	64	69	64	62
77	32	66	64	66	54
80	28	68	56	68	47
83	26	71	48	71	40
87	24	74	42	74	36
92	22	80	38	80	32
95	21	82	36	82	31
99	20	87	34	87	29
105	20	92	33	92	27
112	19	97	32	97	26
153	19	102	32	102	26
204	18	112	30	112	25
306	18	122	29	122	25
408	18	173	29	173	24
510	17	224	28	224	23
700	15	306	28	306	23

Data Interpretation

The measured frequency-dependent complex impedance was converted to the complex electrical conductivity $\sigma^*(\omega)$ using the geometrical factor k of the four-point electrode arrangement:

$$\sigma^*=\frac{1}{\rho^*}=\frac{k}{Z^*}=\frac{l}{A}\frac{1}{Z^*} \quad [4]$$

where Z^* is the measured complex impedance, l is the distance between the two potential electrodes, and A is the cross-sectional area of the column. The complex electrical conductivity can be represented in different manners:

$$\sigma^*(\omega)=\sigma'(\omega)+i\sigma''(\omega)=\left|\sigma^*(\omega)\right|e^{i\varphi(\omega)} \quad [5]$$

where $\omega = 2\pi f$ is the angular frequency and f is the frequency of the applied electrical current, σ' and σ'' are the real and imaginary part of the complex electrical conductivity, $|\sigma^*|$ is the magnitude of the complex conductivity, and $\varphi = \arctan(\sigma''/\sigma')$ is the phase angle. Different methods are available to summarize the measured frequency-dependent complex electrical conductivity. In recent work, the Debye-decomposition approach by Nordsiek and Weller (2008) was widely used for post-processing of SIP measurements. However, the SIP measurements on unsaturated sand–biochar mixtures showed a significant polarization at 1 mHz. In this case, the Debye decomposition cannot capture the entire spectrum (Weigand and Kemna, 2016) and will underestimate the area below the SIP spectrum. Therefore, it is preferred to visually fit a simple Cole–Cole model (Cole and Cole, 1941) to the low-frequency peak of the SIP measurements to characterize the measured complex electrical conductivity:

$$\begin{aligned}\sigma^*(\omega)&=\sigma_\infty\left[1+\frac{M}{1+(i\omega\tau_0)^c}\right]\\&=\sigma_0\left\{1+\frac{M}{1-M}\left[1-\frac{M}{1+(i\omega\tau_0)^c}\right]\right\}\end{aligned} \quad [6]$$

where σ_∞ is the conductivity for infinitely high frequency, σ_0 is the DC conductivity, τ_0 is the relaxation time that directly corresponds to a relaxation frequency f_{rel}, $M = (\sigma_\infty - \sigma_0)/\sigma_\infty$ is the chargeability, which is a measure of the magnitude of polarization, and c is the Cole–Cole exponent that determines the broadness of the relaxation time distribution. The normalized chargeability is commonly defined as $M_n = M/\rho_0$, where ρ_0 is the electrical resistivity (i.e., the inverse of the DC electrical conductivity). Some studies have argued that M_n is more suitable to characterize the polarization of porous media (e.g., Lesmes and Frye, 2001; Weller et al., 2010). Measurement of SIP on saturated samples showed that the M_n of sand–biochar mixtures falls between that of sand–clay and sand–metal mixtures (Gao et al., 2017). However, M_n was found to increase nearly linearly with the electrical conductivity of the pore fluid, which is highly variable in agricultural soils where biochar is anticipated to be applied. Therefore, we used M instead of M_n in this study, as also suggested by Revil et al. (2015b).

Results

Water Retention Characteristics of Sand–Biochar Mixtures

Figure 2a shows the dependence of the water content (θ) of the sand and the two sand–biochar mixtures on the matric potential during pressure drainage. With increasing suction, the θ of sand showed a steep decrease that started at a matric potential of −55 cm. This initial drainage is associated with the air-entry pressure of the largest pore. In the matric potential range between −55 and −80 cm, almost the entire pore space was drained. This indicates a narrow pore size distribution as expected for the well-sorted sand used here. Beyond a matric potential of −80 cm, the θ of sand hardly decreased anymore. The water retention curve for sand was adequately described by the van Genuchten model (Fig. 2a), and the resulting parameters are provided in Table 2. These hydraulic parameters for sand are similar to those reported by Bechtold et al. (2011) for a different sample of the same type of sand.

The water retention characteristics of the two sand–biochar mixtures showed a relatively similar behavior to the pure sand. However, the water content of the saturated sand–biochar mixtures was larger than that of the saturated sand and increased with an increasing amount of biochar. In addition, the water content of the sand–biochar mixtures showed a somewhat earlier decrease around a matric potential of −50 cm, and increasing residual water content due to the addition of biochar. However, it is important to note that the residual water content of the 2% sand–biochar mixture was lower than that of the 1% sand–biochar mixture. This is not consistent with previous work. For example, Amoakwah et al. (2017), Głąb et al. (2016), and Trifunovic et al. (2018) found a positive correlation between the amount of added biochar and the residual water content for most of the investigated samples. The 1% sample was found to be affected by erroneous data at higher absolute values of matric potential which will be discussed below.

Table 2. Fitted model parameters for the water retention curve of sand and biochar.

	Parameters of the van Genuchten model†				
Material	θ_s	θ_r	α	n	m
	——— % ———		cm^{-1}		
Pure sand	40	7	0.015	15.4	0.94
Pure biochar	81	44	0.018	13.0	0.92

† θ_s, saturated soil water content; θ_r, residual soil water content; α, inverse of the air-entry value; n, shape factor related to the pore size distribution; $m = 1 - 1/n$.

In a next step, the dual-porosity model was fitted to the measured data of the 2% sand–biochar mixture using the estimated volume fraction of biochar (10%). The hydraulic parameters determined for pure sand (Table 2) were held constant, and only the hydraulic parameters of the biochar were fitted. The resulting hydraulic parameters of biochar are provided in Table 2, and Fig. 2a presents the fit of the dual-porosity model to the experimental data. In addition, Fig. 2b shows the estimated water retention curves for pure sand and pure biochar. The fitted hydraulic parameters suggest that the biochar particles are highly porous and have a saturated water content of ~81%. This value is close to the estimated porosity of the biochar particles (83%), which is expected since the saturated water content and porosity estimates were obtained from the same weight data. In addition, the fitted residual water content of the biochar was high with 44%, indicating a significant microporosity that remains saturated even for high matric potentials. In addition, the air-entry pressure was found to be lower (higher α) and the pore size distribution somewhat broader (lower n) for biochar than for sand. This explains the broader range of pressures with significant drainage of the sand–biochar mixtures. These findings can be summarized with the conceptual model presented in Fig. 3, which is well supported by the available literature on biochar (Bikbulatova et al., 2018). Figure 3 shows a biochar

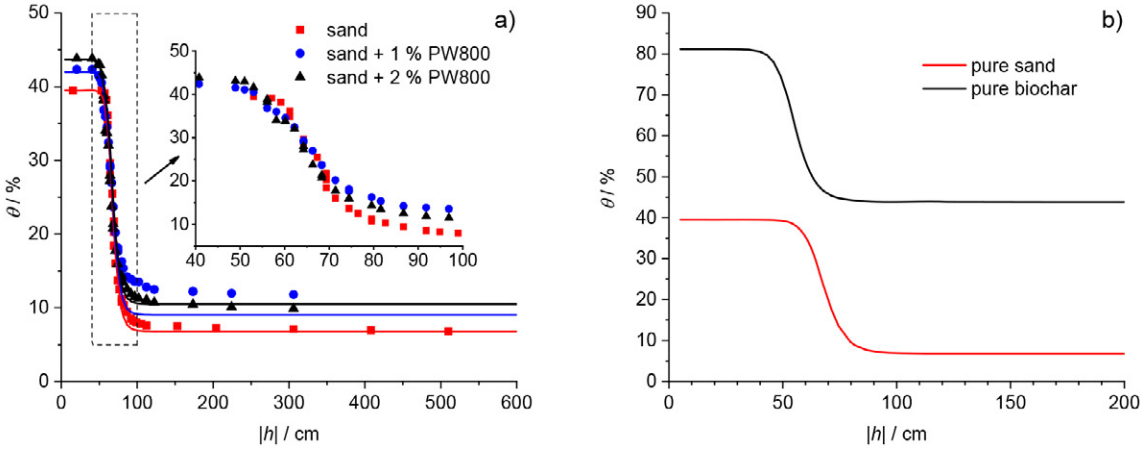

Fig. 2. Water retention characteristics describing the relationship between water content (θ) and matric potential (h) for pure sand and the two sand–biochar mixtures with 1% and 2% biochar; (a) measured values and fits according to Eq. [2] and [3] using the curves from Fig. 2b for pure sand and pure biochar; (b) fit for pure sand by Eq. [2] and modeled curve for pure biochar according to Eq. [2] and [3] from the fit for the 2% sample. PW800 is biochar made by pyrolysis at 800°C from pine wood.

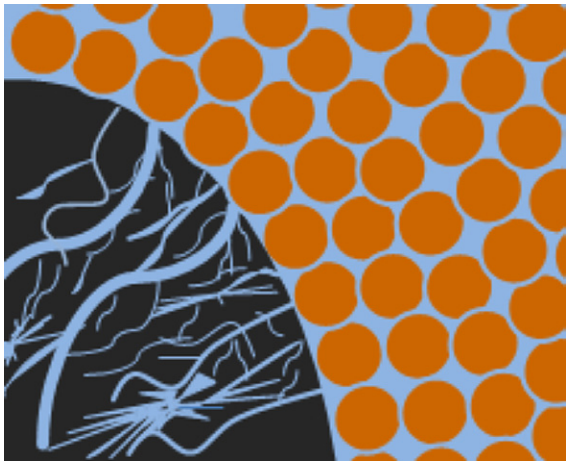

Fig. 3. Conceptual illustration of different types of porosity present in sand–biochar mixtures. Orange indicates sand particles that result in a relatively narrow pore size distribution, whereas the black area indicates biochar with a heterogeneous pore size distribution with both large and small pores.

particle with large and small pores surrounded by spherical sand particles with relatively uniform large pores between them.

The radius r_{min} of the smallest pores, which can be drained at a matric potential of $h = -300$ cm (i.e., the maximum suction applied to the sand–biochar mixtures), can be calculated from the Young–Laplace equation:

$$r_{min} = \frac{2\gamma\cos\theta}{\rho_w g h} \quad [7]$$

A radius of 4.9 μm was obtained with the surface tension of water, $\gamma = 0.0727$ kg s^{-2}, the density of water $\rho_w = 1000$ kg m^{-3}, the gravity constant $g = 9.81$ m s^{-2}, and a wetting angle $\vartheta = 0°$ (complete wetting). For wetting angles larger than 0, which is rather probable for biochars, smaller radii will be obtained. This pore size matches well the characteristic pore size of biochars measured by mercury intrusion (Lu and Zong, 2018).

The previous results are based on the analysis of the results for the 2% sand–biochar mixture. The predicted water retention curve for the 1% sand–biochar mixture using the hydraulic parameters in Table 2 and the estimated volume fraction of biochar (6%) are also provided in Fig. 2a. For low matric potentials, the predicted water content matched the measured water content relatively well, but the quality of the fit deteriorated for higher matric potentials. It is important to note that the measured residual water content at high matric potential is underestimated even when it is assumed that the biochar particles remain fully saturated throughout the drainage experiment. Therefore, it was concluded that the measured water retention curve for the 1% sand–biochar mixture is not physically plausible, and that these data should be used with care when they are used to analyze the relationship between complex electrical conductivity and saturation. The physically implausible results are attributed to an unidentified error in the outflow measurements for the 1% sand–biochar during drainage (e.g., undetected leakage, calibration drift in the pressure transducer used to measure water outflow). To not fully discard the complex electrical conductivity measurements for the 1% sand–biochar mixture, the saturation of the 1% sand–biochar mixture was estimated from the modeled instead of the measured water retention curve in the results below. Obviously, this is a crude approximation, and therefore the results for the electrical measurements on the 1% sand–biochar mixture can only be interpreted in a qualitative manner.

Spectral Induced Polarization Measurements

The measured frequency-dependent complex electrical conductivity of the sand and sand–biochar mixtures for varying water saturation is presented in Fig. 4 for frequencies between 1 mHz and 1 kHz. Data for higher frequencies were deleted because of the increasing importance of capacitive errors with increasing desaturation (Huisman et al., 2016). In a first step, the DC electrical conductivity (σ_0) determined by fitting a Cole–Cole model to the SIP data, will be interpreted as a function of saturation. As expected, σ_0 decreased with decreasing water saturation (Fig. 5).

For homogeneous samples like the sand sample used in this study, the σ_0 of a porous media can be described by the following relationship derived by Linde et al. (2006):

$$\sigma_0 = \frac{1}{F}\sigma_w S_w^{n_1} + \left(\frac{F-1}{F}\right)\sigma'_{surf} \quad [8]$$

$$F = \phi^{-m_1} \quad [9]$$

where F is the formation factor, ϕ is the porosity, m_1 is the cementation exponent, σ_w is the electrical conductivity of the pore electrolyte, n_1 is the saturation exponent, and σ'_{surf} is the real part of the surface conductivity. This model ignores deviations that occur when approaching the percolation threshold (Jougnot et al., 2010), which is expected to be situated at very low saturation for sand. It was able to fit the data for sand reasonably well with the water electrical conductivity used for sample preparation ($\sigma_w = 0.045$ S m^{-1}) (Fig. 5). The fitted model parameters for sand were $F = 3.75$, $m_1 = 1.42$, $n_1 = 2.27$, and $\sigma'_{surf} = 3.92 \times 10^{-15}$ S m^{-1}. The low value for σ'_{surf} is a result of the fitting procedure and just indicates negligible surface conductivity for the pure sand. The formation factor F matches well with a previously reported value for a similar sand (Breede et al., 2011), and the saturation exponent n_1 falls within the range determined by Ulrich and Slater (2004) for a series of different sands.

The relationship between σ_0 and S_w of the sand–biochar mixtures was different from that of sand in two aspects. First, σ_0 at full saturation increased with increasing amount of biochar although the electrical conductivity of the water used for sample preparation was identical. Second, the relationship between $\log(\sigma_0)$ and $\log(S_w)$ was found to be nonlinear for the sand–biochar mixtures, especially in the low saturation range (Fig. 5). Sen (1997) showed that models such as Eq. [8] do not apply for heterogeneous samples with micro- and macroporosity. In particular, the water contained in the micropores may become disconnected when the large pores

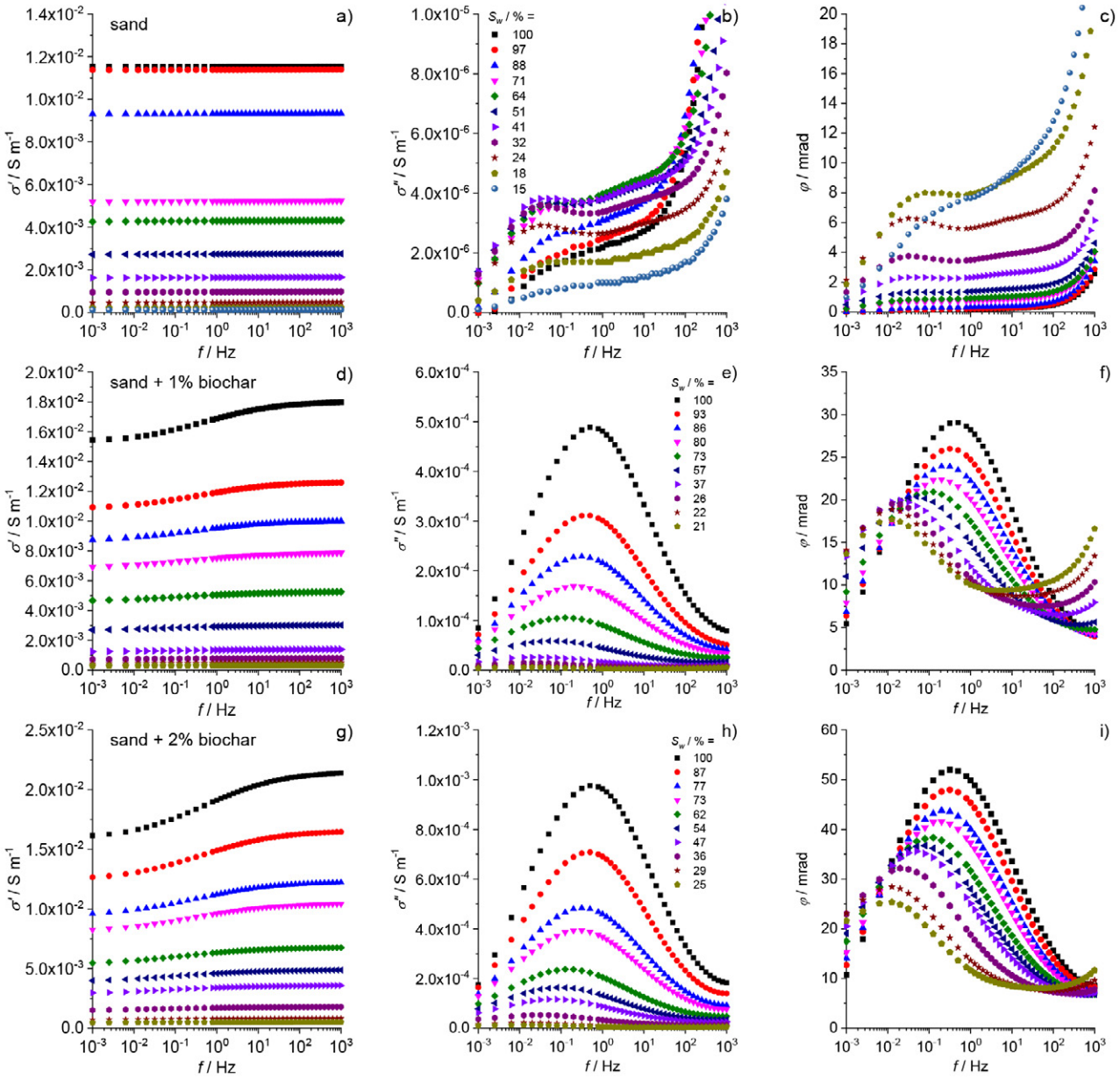

Fig. 4. Spectral induced polarization (SIP) measurements on pure sand (top row), 1% sand–biochar mixture (middle row), and 2% sand–biochar mixture (bottom row) for a range of saturation. The SIP measurements are presented as the real part of the electrical conductivity (σ′, left column), the imaginary part of the electrical conductivity (σ″, middle column), and the phase of the electrical conductivity (φ, right column). The *x* axis shows the frequency (*f*).

are drained and therefore contribute less to the bulk electrical conductivity. For such cases, Sen (1997) argued that the mixing model of Maxwell (1873) can be used if the volume fraction of the inclusions is below the percolation threshold (~18%), which is the case for our sand–biochar mixtures. Therefore, the following model based on Maxwell (1873) was used to describe the σ_0 of unsaturated sand–biochar mixtures (Sen, 1997):

$$\sigma_0 = \sigma_s \frac{2\sigma_s + \sigma_{bio} - 2\upsilon(\sigma_s - \sigma_{bio})}{2\sigma_s + \sigma_{bio} + \upsilon(\sigma_s - \sigma_{bio})} \quad [10]$$

$$\sigma_s = \sigma_w S_{ws}^{n_s} \phi_s^{m_s},\ \sigma_{bio} = \sigma_w S_{wbio}^{n_{bio}} \phi_{bio}^{m_{bio}} \quad [11]$$

where σ_s and σ_{bio} are the saturation-dependent electrical conductivity of the sandy host media and biochar, respectively, υ is the volume fraction of the biochar particles, σ_w is the water electrical conductivity, S_{wi} is the water saturation, n_i is the saturation exponent, m_i is the cementation exponent, ϕ_i is the porosity, and the subscript *i* can either be "s" for the sandy host medium or "bio" for the biochar particles.

For the sand–biochar mixtures, σ_0 as a function of S_w predicted by Eq. [10] and [11] was compared with the available measurements. S_{ws} and S_{wbio} were calculated from the obtained water retention curves (Fig. 2b, Table 2) for each of the applied pressure steps (Table 1). The values of m_s and n_s for the sand

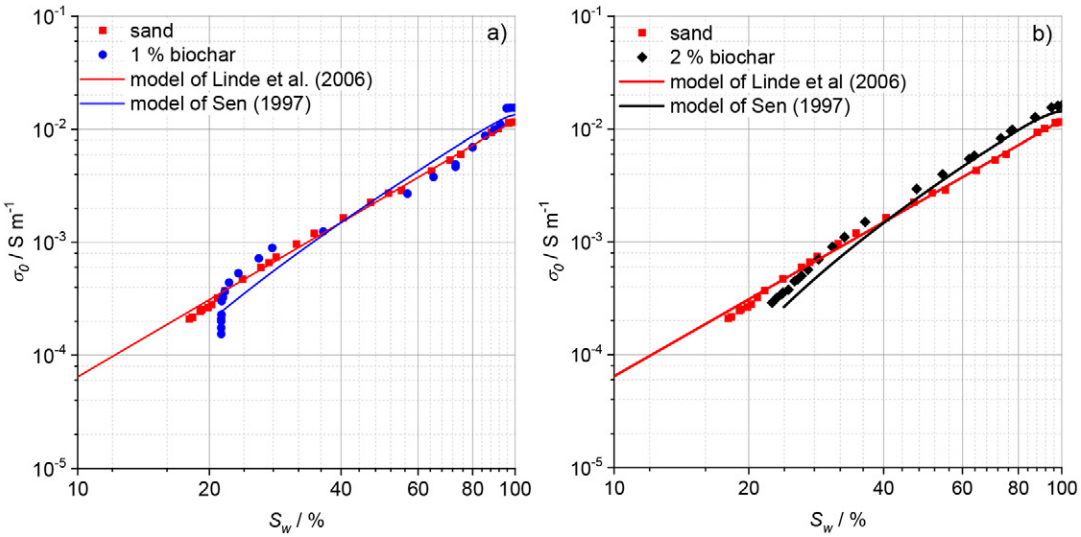

Fig. 5. Direct current electrical conductivity (σ_0) as a function of saturation (S_w) for (a) sand and the 1% sand–biochar mixture and (b) sand and the 2% sand–biochar mixture. The solid red line indicates the model predictions using the model of Linde et al. (2006) for sand, and the blue and black lines indicate the model predictions using the model of Sen (1997) for sand–biochar mixtures.

fraction were assumed to be equal to the fitted values of m_1 and n_1 from the model of Linde et al. (2006) that were obtained for the pure sand sample. This seems a reasonable approximation because of the relatively low volume fraction of biochar. It was also assumed that σ_w was equal to the electrical conductivity of the water used for sample preparation. Finally, the values of n_{bio} and m_{bio} were not known. The saturation exponent was set to the widely used value of 2 following the original work by Archie (1942). The cementation exponent was also set to the value of 2. This is the lower limit for m found by Fang et al. (2018) for coal using gas diffusion measurements. The model showed a reasonable fit to the measured σ_0 for the 2% sand–biochar mixtures (Fig. 5b). In particular, the nonlinearity in the log–log representation of the data is well captured. However, the model seems to underestimate σ_0 for the entire range of saturation. This is at least partly related to a probable underestimation of σ_w due to a release of adsorbed ions from the biochar during sample preparation. The fit to the measured data could be slightly improved by fitting σ_w to the measured data (result not shown), which resulted in a value of $\sigma_w = 0.055$ S m^{-1} instead of the value of 0.045 S m^{-1} for the 4 mM NaCl solution used during sample preparation. This is an increase of 22%. In previous work, σ_0 was found to be 0.0140 S m^{-1} for a sample with the same composition and similar porosity when it was flushed with 4 mM NaCl solution. The value of σ_0 at full saturation determined in this study was 14% larger. The model fit to the measurements of the 1% sand–biochar mixture is shown in Fig. 5a. Clearly, the model fit is of much lower quality, which is attributed to the considerable uncertainty in the saturation of this sand-biochar mixture as explained in the previous section.

In a next step, $\sigma''(\omega)$ as well as the fitted total chargeability and Cole–Cole exponent were analyzed. The $\sigma''(\omega)$ and $\phi(\omega)$ of sand showed a weak maximum in the low-frequency range around 0.01 to 0.1 Hz for partially saturated conditions and a strong increase in the high-frequency range with desaturation (Fig. 4b and 4c). The $\sigma''(\omega)$ in the millihertz to hertz frequency range first increased and then decreased with decreasing water saturation. The maximum value for $\sigma''(\omega)$ in this frequency range was obtained for a water saturation of ~45%. These results for sand agree well with the results of Breede et al. (2012), who used similar sand and the same experimental method. Breede et al. (2012) proposed a conceptual model to explain how desaturation affects the SIP spectra of sand based on the short-narrow pore model (Titov et al., 2002). Their explanation suggests that the grain contact areas act as the short-narrow pore at full saturation. With increasing desaturation, the large inter-grain pores that are the dominant pathway of electrical current for the saturated sample release water while the grain contact regions remain wet. Therefore, the remaining water films around the particle become the narrow pores that connect the thicker water films at the grain contact areas for electrical current flow. This results in a decrease of the ohmic conductivity and an increase of polarization. With progressing drainage, the difference in thickness between the water films in the grain contact area and around the particles decreases, therefore, both the magnitude and phase of $\sigma^*(\omega)$ decrease. The increase of $\sigma''(\omega)$ and $\phi(\omega)$ for frequencies above 100 Hz is related to the increasing contact impedance of the potential electrodes with decreasing saturation (Huisman et al., 2016), and to Maxwell–Wagner polarization of the porous media (Breede et al., 2012).

The shape of the measured $\sigma'(\omega)$ and $\sigma''(\omega)$ is similar for the mixtures with 1% biochar (Fig. 4d and 4e) and 2% biochar (Fig. 4g and 4h). The $\sigma'(\omega)$ increased with increasing frequency and approached a plateau. The increase in conductivity with frequency was stronger for the sand–biochar mixture with 2% biochar than for the mixture with 1% biochar. Accordingly, a peak was found in $\sigma''(\omega)$ and $\phi(\omega)$, which is consistent with the Kramers–Kronig relationship that describes the coupling between $\sigma'(\omega)$, $\sigma''(\omega)$, and

$\phi(\omega)$ (Toll, 1956). The total chargeability (M) and the Cole–Cole exponent (c) as a function of saturation are presented in Fig. 6 and 7 for the two sand–biochar mixtures. The M values obtained for the 1% and 2% sand–biochar mixtures ranged from 0.11 to 0.16 and 0.16 to 0.28, respectively. In addition, M decreased continuously with decreasing saturation as expected from the decreasing size of the peak in $\phi(\omega)$ (Fig. 4f and 4i). It decreased fast between 95 and 75% and thereafter decreased slower until a water saturation of 40%. In the low-saturation range, the decrease in M with decreasing saturation became faster again. The fitted c values for the two sand–biochar mixtures varied slightly between 0.34 and 0.43 and were slightly less than those found by Maineult et al. (2018) for pore network modeling. In contrast with the results of Maineult et al. (2018), c decreased with desaturation (Fig. 7) for our samples, which reflects the increasing influence of the background of the matrix. Again, the behavior of the 1% sand–biochar mixture should be interpreted with care due to the uncertainty in the saturation.

The polarization of the sand–biochar mixture can, in principle, also be interpreted by applying the mixing model presented in Eq. [10] for the whole frequency range (e.g., see the reformulated Eq. [13] in Revil et al., 2015b). In the simple case of a nondraining conductive particle in a nonpolarizing sand background, it can be shown that the chargeability will decrease with decreasing saturation (i.e., decreasing electrical conductivity). The same trend can also be seen from the measurements with variable water electrical conductivity but the same amount of biochar presented in Gao et al. (2017). However, a more quantitative analysis using mixing models is currently hampered by the need to estimate $\sigma^*(\omega)$ as a function of saturation for both the sand and the biochar fraction. In qualitative terms, it is observed that the drainage of the large pores led to an initially strong decrease in the chargeability in the high saturation range, which may be explained by the loss of continuity in the water film within and around the particles of biochar. With increasing desaturation, the polarization of the sandy host media is increasing while the polarization of the biochar further decreases. This opposite behavior becomes significant when $\sigma''(\omega)$ of the sand–biochar mixtures decreases to a comparable order of magnitude as the sand. This may explain the reduced decrease of chargeability for intermediate saturation between 75 and 40%. With progressing drainage, the polarization of sand starts to decrease, resulting in a stronger decrease in the polarization of the sand–biochar mixtures.

In a final step, the dependence of the relaxation time (τ_0) on saturation was analyzed. Figure 4 indicates that the peak frequency

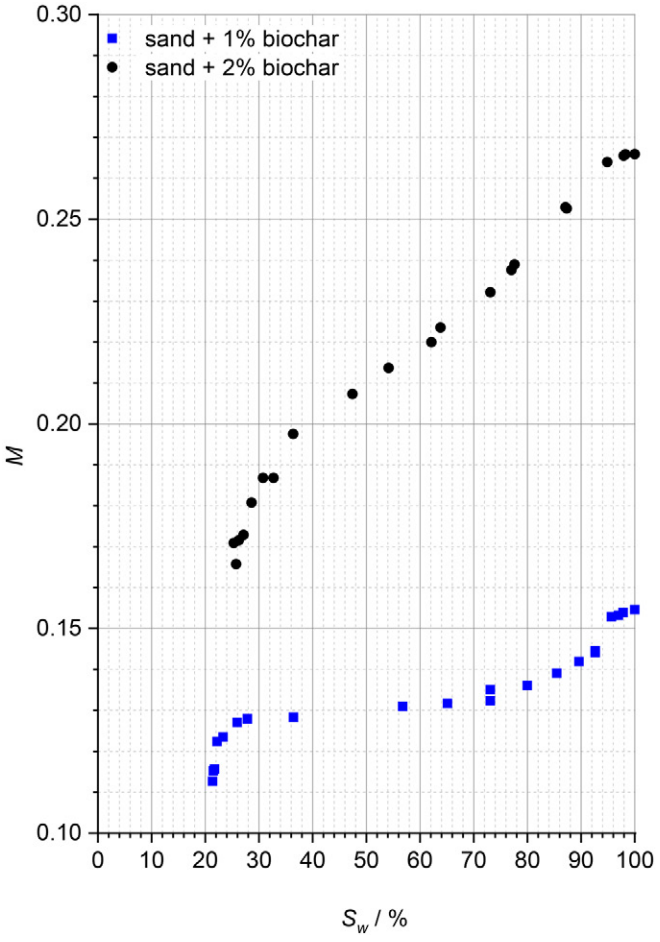

Fig. 6. Total chargeability (M) as a function of saturation (S_w) obtained by fitting a Cole–Cole model to spectral induced polarization (SIP) data for the 1 and 2% sand–biochar mixtures.

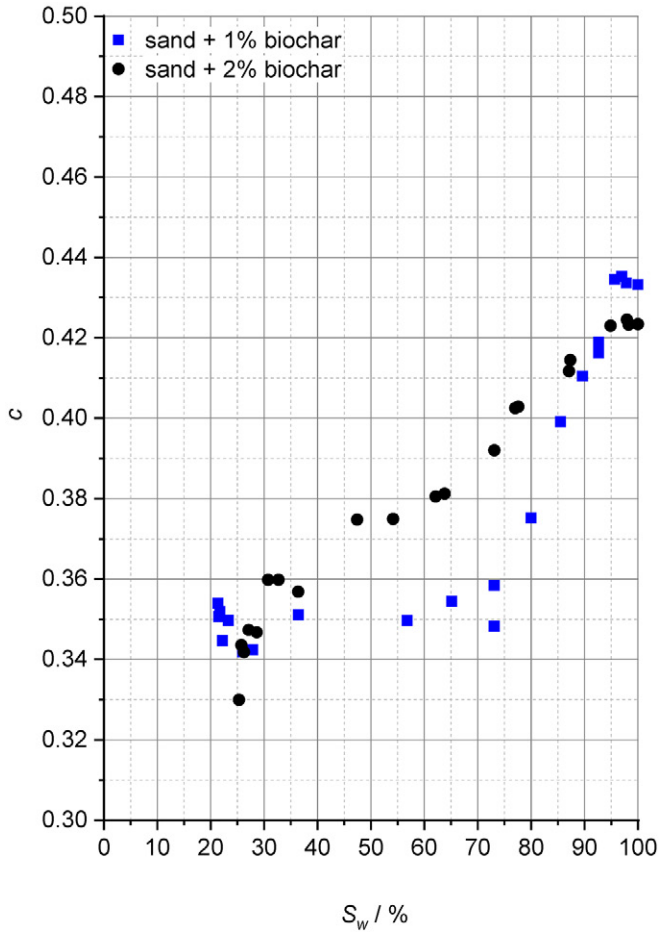

Fig. 7. Cole–Cole exponent (c) as a function of saturation (S_w) obtained by fitting a Cole–Cole model to spectral induced polarization (SIP) data for the 1 and 2% sand–biochar mixtures.

shifted to lower frequencies with decreasing saturation for both sand–biochar mixtures. The τ_0 derived from fitting the Cole–Cole model is presented in Fig. 8 as a function of S_w. It was found that the τ_0 increased with decreasing saturation, which is the opposite direction as observed for unsaturated sand without conductive particles (Breede et al., 2012) and modeling results on pore networks without conductive particles (Maineult et al., 2018). The values for τ_0 varied from 0.3 s for saturated sand–biochar mixtures to ~20 s for sand–biochar mixtures with a saturation of 0.26. The sand–biochar mixtures with 2% biochar showed a linear relationship between $\log(\tau_0)$ and $\log(S_w)$ with a slope of −3.17, whereas the sand–biochar mixtures with 1% biochar showed a somewhat nonlinear relationship but the same general trend. In a range of studies, the relaxation time (τ_0) was described as a function of particle radius r and a diffusion coefficient D (Gurin et al., 2015; Leroy et al., 2008; Schwarz, 1962):

$$\tau_0 = \frac{r^2}{2D} \quad [12]$$

Based on modeling work of EDL polarization by Schwarz (1962), Leroy et al. (2008) suggested that D is the diffusion coefficient of the counter-ions in the Stern layer. For conductive particles, Gurin et al. (2013) suggested that D is an apparent diffusion coefficient of the charge carriers responsible for the polarization dependent on both the particle mineralogy and surface chemistry. Revil et al. (2015b) suggested that D is related to the diffusion coefficient of charge carriers inside the particle. In the case of the sand–biochar mixtures, the increasing τ_0 with decreasing saturation can potentially be explained by a decrease of the apparent diffusion coefficient of ions due to desaturation of the biochar particles. Kastening and Heins (2005) reported that the ionic diffusion coefficient in micropores of active carbon is about one order of magnitude smaller than in the macropores due to restricted movement within the strongly overlapping EDL of opposing pore walls and the surface chemical properties of active carbon. This decreasing diffusion coefficient may explain the fundamental difference to the results on the modeling of pore networks assuming constant diffusion coefficients for all pores with a mean radius of 10 μm (Maineult et al., 2018). It should also be noted that the peak frequency of $\phi(\omega)$ of the sand–biochar mixtures approached that of the pure sand for low saturation (Fig. 4), which might suggest that the polarization of biochar is very weak at low saturation.

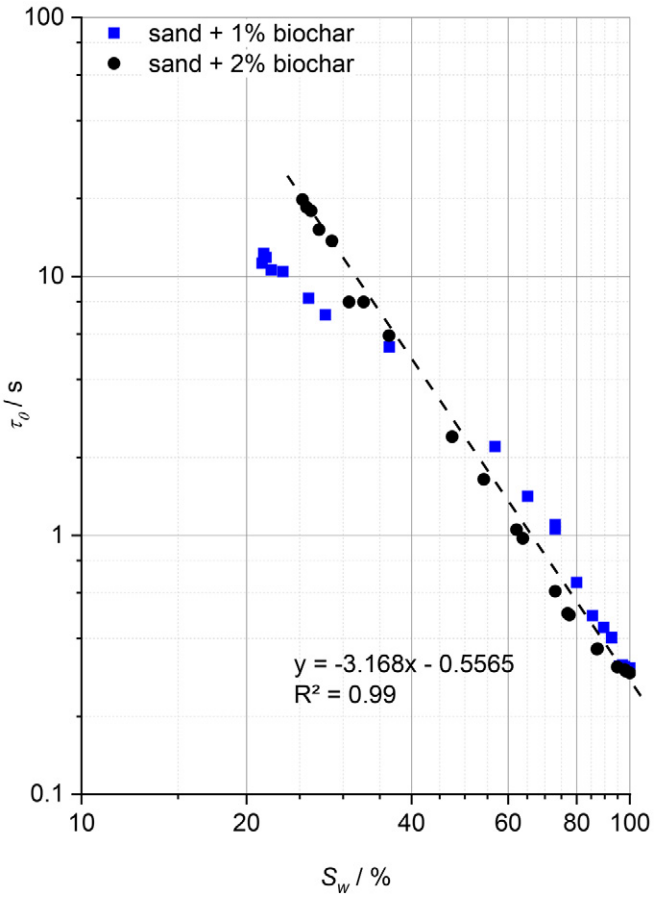

Fig. 8. Relaxation time (τ_0) as a function of saturation (S_w) obtained by fitting a Cole–Cole model to spectral induced polarization (SIP) data for the 1 and 2% sand–biochar mixtures and linear fit for the 2% sand–biochar mixture.

Discussion

Based on the SIP measurements on saturated sand–biochar mixtures in Gao et al. (2017) and the measurements on partially saturated samples in this study, it can be concluded that biochar shows a relatively strong polarization that is comparable to conductive materials. For full saturation where the inner pores of biochar are saturated and connected, it was found that $\phi(\omega)$ and M mainly depend on the amount of biochar, and that τ_0 depends on the particle size of biochar and on the electrical conductivity of the water in the porous media. The relationships found for saturated conditions were consistent with measurements (Placencia-Gómez and Slater, 2016; Revil et al., 2015a) and modeling (Gurin et al., 2015; Revil et al., 2015b; Wong, 1979) of porous media with conductive particles. In the case of unsaturated sand–biochar mixtures, the highly porous nature of biochar played an important role in understanding the experimental results. The water retention curves of the sand–biochar mixtures were interpreted using a dual-porosity model, and it was found that the biochar particles consist of a macroporosity that drained in a similar pressure range as the sand and a relatively large microporosity that remained saturated in the pressure range considered in this study. At high suction, biochar particles with a considerable amount of residual water were dispersed in a dry sand background. This resulted in a nonlinear dependence of $\sigma'(\omega)$ on saturation in a log–log representation that could be described with a dielectric mixing model of Maxwell (1873). The drainage of the biochar particles probably also explains the steep decrease of $\phi(\omega)$ and M and the continuous increase of τ_0 with decreasing saturation.

The results in this study phenomenologically illustrate the dependence of the complex electrical conductivity of sand and sand–biochar mixtures on saturation. However, there is still a lack

of understanding of mechanistic principles that determine the SIP response of biochar particles in porous media. The mechanistic understanding of polarization processes in partially saturated media is even less well developed. Studies of the SIP response of unsaturated porous media with conductive particles are even rarer, and to the best of our knowledge, this is the first study that considers porous conducting particles. A promising approach might be the modeling of pore networks (Maineult et al., 2018), which, however, requires suitable models for the polarization of single pores in conductive particles. Therefore, there is a clear need to increase the database of SIP measurements on partially saturated porous media with and without addition of conductive particles. Gao et al. (2017) suggested that the polarization of biochar in saturated media is related to the electric polarization of the biochar particle itself and the polarization of the EDL around the particle. However, available mechanistic models for the polarization of conductive particles (Gurin et al., 2015; Revil et al., 2015b; Wong, 1979) are not adequate to quantitatively analyze the polarization in the complex case of drainable biochar particles in a polarizing background medium. An improved mechanistic model needs to be developed to make progress here.

The results presented in Gao et al. (2017) and in this study generally confirm that there is a considerable contrast between the SIP response of sand and sand–biochar mixtures. Comparing the scale of Fig. 4c (sand) with that of Fig. 4f and 4i (sand–biochar mixtures), it can be seen that the maximum phase value for the 1% sand–biochar mixture is more than two times higher than for sand. Revil et al. (2015b) concluded that the signals of conductive particles and a weakly polarizing background are additive. Therefore, it is expected that field SIP imaging of the complex conductivity distribution allows a qualitative distinction of soil with and without biochar. This may already be useful to evaluate depth and homogeneity of biochar application in field studies. For a more quantitative use of SIP measurements for assessing the spatial variability of biochar amendments, an important question is whether variations in biochar amount can be distinguished in the presence of variability in water saturation. In general, the water saturation of agricultural soils is in a range between 20 and 70%. With applied amounts of 1 and 2% biochar, the sand–biochar mixtures investigated in this study showed a stronger polarization even for a saturation of 25% (Fig. 4f and 4i) compared with pure sand. In addition, the observed phase values for the unsaturated sand-biochar mixtures (i.e., above 15 and 20 mrad, respectively, even for relatively dry mixtures in the millihertz to hertz frequency range) were considerably higher than the phase values observed for unsaturated soils in other studies, which typically reported phase values below 10 mrad in this low-frequency range (e.g., Ghorbani et al., 2008; Kelter et al., 2018). This provides confidence that biochar with similar properties as PW800 can also be detected in unsaturated soils at application rates of 20 to 50 t ha^{-1} (0.5–3 mass %, depending on the depth of mixing with soil) used in many field trials (Ding et al., 2016; Mukherjee and Lal, 2014). If the hydraulic and electrical properties of biochar can be characterized using laboratory investigations before the field application of biochar, it may also be possible to quantify the amount of biochar. For example, the sand–biochar mixtures investigated in this study showed a strong dependence of the relaxation time on the saturation but not on the amount of biochar, which potentially allows separation of these effects.

Conclusions

The SIP response of sand–biochar mixtures is larger than that of sand in the entire saturation range found in agricultural soil. The polarization of the mixtures approaches that of sand with decreasing water content, but the difference can still be well quantified at low saturation, allowing the distinction of soil with and without biochar. For biochars of the type used in this study, the effect seems to be large enough to be also quantified in real soil, but this needs to be investigated in more detail. The characteristics of the spectral response of biochar in soil at varying water content can potentially be used to discriminate spatial variation of biochar and water content in field experiments. In a next step, we aim to verify the suitability of SIP for monitoring the influence of biochar on the water content of soil at a larger scale. Overall, field SIP measurements are considered to be a promising tool for the characterization and monitoring of biochar amendments to agricultural soils. They may provide a means for the determination of changes in the influence of biochar on soil properties due to aging, which is an important question currently investigated.

The results of the present study also provide useful information for the development and validation of models describing the complex electrical conductivity of porous media with conductive and semiconductive particles (Bücker et al., 2018; Revil et al., 2015b). The observed increase of relaxation times with progressive desaturation could perhaps be investigated using the pore network modeling approach of Maineult et al. (2018) with varying diffusion coefficients. In an even broader context, the results presented here could also support electrochemical investigations and models for carbon electrodes used in supercapacitors (Kastening and Heins, 2005).

Acknowledgments

Zhan Gao would like to thank the Chinese Scholarship Council for financial support of his Ph.D. thesis.

References

Agegnehu, G., A.K. Srivastava, and M.I. Bird. 2017. The role of biochar and biochar–compost in improving soil quality and crop performance: A review. Appl. Soil Ecol. 119:156–170. doi:10.1016/j.apsoil.2017.06.008

Amoakwah, E., K.A. Frimpong, D. Okae-Anti, and E. Arthur. 2017. Soil water retention, air flow and pore structure characteristics after corn cob biochar application to a tropical sandy loam. Geoderma 307:189–197. doi:10.1016/j.geoderma.2017.08.025

Archie, G.E. 1942. The electrical resistivity log as an aid in determining some reservoir characteristics. Trans. Am. Inst. Min. Metall. Eng. 146:54–61. doi:10.2118/942054-G

Arthur, E., and F. Ahmed. 2017. Rice straw biochar affects water retention and air movement in a sand-textured tropical soil. Arch. Agron. Soil Sci. 63:2035–2047. doi:10.1080/03650340.2017.1322196

Bechtold, M., S. Haber-Pohlmeier, J. Vanderborght, A. Pohlmeier, T.P.A. Ferré, and H. Vereecken. 2011. Near-surface solute redistribution during evaporation. Geophys. Res. Lett. 38:L17404. doi:10.1029/2011GL048147

Bikbulatova, S., A. Tahmasebi, Z.Q. Zhang, S.K. Rish, and J.L. Yu. 2018. Understanding water retention behavior and mechanism in bio-char. Fuel Process. Technol. 169:101–111. doi:10.1016/j.fuproc.2017.09.025

Binley, A., L.D. Slater, M. Fukes, and G. Cassiani. 2005. Relationship between spectral induced polarization and hydraulic properties of saturated and unsaturated sandstone. Water Resour. Res. 41:W12417. doi:10.1029/2005WR004202

Breede, K., A. Kemna, O. Esser, E. Zimmermann, H. Vereecken, and J.A. Huisman. 2011. Joint measurement setup for determining spectral induced polarization and soil hydraulic properties. Vadose Zone J. 10:716–726. doi:10.2136/vzj2010.0110

Breede, K., A. Kemna, O. Esser, E. Zimmermann, H. Vereecken, and J.A. Huisman. 2012. Spectral induced polarization measurements on variably saturated sand–clay mixtures. Near Surf. Geophys. 10:479–489. doi:10.3997/1873-0604.2012048

Bücker, M., A. Flores Orozco, and A. Kemna. 2018. Electrochemical polarization around metallic particles—Part 1: The role of diffuse-layer and volume-diffusion relaxation. Geophysics 83:E203–E217. doi:10.1190/geo2017-0401.1

Cha, J.S., S.H. Park, S.C. Jung, C. Ryu, J.K. Jeon, M.C. Shin, and Y.K. Park. 2016. Production and utilization of biochar: A review. J. Ind. Eng. Chem. 40:1–15. doi:10.1016/j.jiec.2016.06.002

Cole, K.S., and R.H. Cole. 1941. Dispersion and absorption in dielectrics I. Alternating current characteristics. J. Chem. Phys. 9:341–351. doi:10.1063/1.1750906

Ding, Y., Y.G. Liu, S.B. Liu, Z.W. Li, X.F. Tan, X.X. Huang, et al. 2016. Biochar to improve soil fertility. A review. Agron. Sustain. Dev. 36:36. doi:10.1007/s13593-016-0372-z

Fang, X.L., Y.D. Cai, D.M. Liu, and Y.F. Zhou. 2018. A mercury intrusion porosimetry method for methane diffusivity and permeability evaluation in coals: A comparative analysis. Appl. Sci. 8:860. doi:10.3390/app8060860

Gao, Z., F.-H. Haegel, J.A. Huisman, O. Esser, E. Zimmermann, and H. Vereecken. 2017. Spectral induced polarization for the characterisation of biochar in sand. Near Surf. Geophys. 15:645–656. doi:10.3997/1873-0604.2017045

Ghorbani, A., P. Cosenza, S. Ruy, C. Doussan, and N. Florsch. 2008. Non-invasive monitoring of water infiltration in a silty clay loam soil using spectral induced polarization. Water Resour. Res. 44:W08402. doi:10.1029/2007WR006114

Głąb, T., J. Palmowska, T. Zaleski, and K. Gondek. 2016. Effect of biochar application on soil hydrological properties and physical quality of sandy soil. Geoderma 281:11–20. doi:10.1016/j.geoderma.2016.06.028

Grunat, D.A., L.D. Slater, and M. Wehrer. 2013. Complex electrical measurements on an undisturbed soil core: Evidence for improved estimation of saturation degree from imaginary conductivity. Vadose Zone J. 12(4). doi:10.2136/vzj2013.03.0059

Gurin, G., A. Tarasov, Y. Ilyin, and K. Titov. 2013. Time domain spectral induced polarization of disseminated electronic conductors: Laboratory data analysis through the Debye decomposition approach. J. Appl. Geophys. 98:44–53. doi:10.1016/j.jappgeo.2013.07.008

Gurin, G., K. Titov, Y. Ilyin, and A. Tarasov. 2015. Induced polarization of disseminated electronically conductive minerals: A semi-empirical model. Geophys. J. Int. 200:1555–1565. doi:10.1093/gji/ggu490

Huisman, J.A., E. Zimmermann, O. Esser, F.-H. Haegel, A. Treichel, and H. Vereecken. 2016. Evaluation of a novel correction procedure to remove electrode impedance effects from broadband SIP measurements. J. Appl. Geophys. 135:466–473. doi:10.1016/j.jappgeo.2015.11.008

Hupfer, S., T. Martin, A. Weller, T. Günther, K. Kuhn, V.D.N. Ngninjio, and U. Noell. 2016. Polarization effects of unconsolidated sulphide–sand-mixtures. J. Appl. Geophys. 135:456–465. doi:10.1016/j.jappgeo.2015.12.003

Jougnot, D., A. Ghorbani, A. Revil, P. Leroy, and P. Cosenza. 2010. Spectral induced polarization of partially saturated clay-rocks: A mechanistic approach. Geophys. J. Int. 180:210–224. doi:10.1111/j.1365-246X.2009.04426.x

Kastening, B., and M. Heins. 2005. Properties of electrolytes in the micropores of activated carbon. Electrochim. Acta 50:2487–2498. doi:10.1016/j.electacta.2004.10.077

Kavitha, B., P.V.L. Reddy, B. Kim, S.S. Lee, S.K. Pandey, and K.H. Kim. 2018. Benefits and limitations of biochar amendment in agricultural soils: A review. J. Environ. Manage. 227:146–154. doi:10.1016/j.jenvman.2018.08.082

Kelter, M., J.A. Huisman, E. Zimmermann, and H. Vereecken. 2018. Field evaluation of broadband spectral electrical imaging for soil and aquifer characterization. J. Appl. Geophys. 159:484–496. doi:10.1016/j.jappgeo.2018.09.029

Kemna, A., A. Binley, G. Cassiani, E. Niederleithinger, A. Revil, L. Slater, et al. 2012. An overview of the spectral induced polarization method for near-surface applications. Near Surf. Geophys. 10:453–468. doi:10.3997/1873-0604.2012027

Kuppusamy, S., P. Thavamani, M. Megharaj, K. Venkateswarlu, and R. Naidu. 2016. Agronomic and remedial benefits and risks of applying biochar to soil: Current knowledge and future research directions. Environ. Int. 87:1–12. doi:10.1016/j.envint.2015.10.018

Leroy, P., A. Revil, A. Kemna, P. Cosenza, and A. Ghorbani. 2008. Complex conductivity of water-saturated packs of glass beads. J. Colloid Interface Sci. 321:103–117. doi:10.1016/j.jcis.2007.12.031

Lesmes, D.P., and K.M. Frye. 2001. Influence of pore fluid chemistry on the complex conductivity and induced polarization responses of Berea sandstone. J. Geophys. Res. 106(B3):4079–4090. doi:10.1029/2000JB900392

Linde, N., A. Binley, A. Tryggvason, L.B. Pedersen, and A. Revil. 2006. Improved hydrogeophysical characterization using joint inversion of cross-hole electrical resistance and ground-penetrating radar traveltime data. Water Resour. Res. 42:W12404. doi:10.1029/2006WR005131

Lu, S.G., and Y.T. Zong. 2018. Pore structure and environmental serves of biochars derived from different feedstocks and pyrolysis conditions. Environ. Sci. Pollut. Res. Int. 25:30401–30409. doi:10.1007/s11356-018-3018-7

Maineult, A., D. Jougnot, and A. Revil. 2018. Variations of petrophysical properties and spectral induced polarization in response to drainage and imbibition: A study on a correlated random tube network. Geophys. J. Int. 212:1398–1411. doi:10.1093/gji/ggx474

Maxwell, J.C. 1873. Conduction through heterogenous media. In: A treatise on electricity and magnetism. Vol. I. Clarendon Press, Oxford, UK. p. 360–373. http://www.aproged.pt/biblioteca/MaxwellI.pdf (accessed 16 July 2019).

Mukherjee, A., and R. Lal. 2014. The biochar dilemma. Soil Res. 52:217–230. doi:10.1071/SR13359

Nordsiek, S., and A. Weller. 2008. A new approach to fitting induced-polarization spectra. Geophysics 73:F235–F245. doi:10.1190/1.2987412

Placencia-Gómez, E., and L.D. Slater. 2016. On the pore water chemistry effect on spectral induced polarization measurements in the presence of pyrite. J. Appl. Geophys. 135:474–485. doi:10.1016/j.jappgeo.2015.11.001

Revil, A., G.Z.A. Aal, E.A. Atekwana, D.Q. Mao, and N. Florsch. 2015a. Induced polarization response of porous media with metallic particles—Part 2: Comparison with a broad database of experimental data. Geophysics 80:D539–D552. doi:10.1190/geo2014-0578.1

Revil, A., N. Florsch, and D.Q. Mao. 2015b. Induced polarization response of porous media with metallic particles: 1. A theory for disseminated semiconductors. Geophysics 80:D525–D538. doi:10.1190/geo2014-0577.1

Schwarz, G. 1962. A theory of the low-frequency dielectric dispersion of colloidal particles in electrolyte solution. J. Phys. Chem. 66:2636–2642. doi:10.1021/j100818a067

Sen, P.N. 1997. Resistivity of partially saturated carbonate rocks with microporosity. Geophysics 62:415–425. doi:10.1190/1.1444152

Šimůnek, J., N.J. Jarvis, M.Th. van Genuchten, and A. Gärdenäs. 2003. Review and comparison of models for describing non-equilibrium and preferential flow and transport in the vadose zone. J. Hydrol. 272:14–35. doi:10.1016/S0022-1694(02)00252-4

Titov, K., A. Kemna, A. Tarasov, and H. Vereecken. 2004. Induced polarization of unsaturated sands determined through time domain measurements. Vadose Zone J. 3:1160–1168. doi:10.2136/vzj2004.1160

Titov, K., V. Komarov, V. Tarasov, and A. Levitski. 2002. Theoretical and experimental study of time domain-induced polarization in water-saturated sands. J. Appl. Geophys. 50:417–433. doi:10.1016/S0926-9851(02)00168-4

Toll, J.S. 1956. Causality and the dispersion relation: Logical foundations. Phys. Rev. 104:1760–1770. doi:10.1103/PhysRev.104.1760

Trifunovic, B., H.B. Gonzalez, S. Ravi, B.S. Sharratt, and S.K. Mohanty. 2018. Dynamic effects of biochar concentration and particle size on hydraulic properties of sand. Land Degrad. Dev. 29:884–893. doi:10.1002/ldr.2906

Ulrich, C., and L.D. Slater. 2004. Induced polarization measurements on unsaturated, unconsolidated sands. Geophysics 69:762–771. doi:10.1190/1.1759462

van Genuchten, M.Th. 1980. A closed-form equation for predicting the hydraulic conductivity of unsaturated soil. Soil Sci. Soc. Am. J. 44:892–898. doi:10.2136/sssaj1980.03615995004400050002x

Weber, K., and P. Quicker. 2018. Properties of biochar. Fuel 217:240–261. doi:10.1016/j.fuel.2017.12.054

Weigand, M., and A. Kemna. 2016. Relationship between Cole–Cole model parameters and spectral decomposition parameters derived from SIP data. Geophys. J. Int. 205:1414–1419. doi:10.1093/gji/ggw099

Weller, A., L. Slater, S. Nordsiek, and D. Ntarlagiannis. 2010. On the estimation of specific surface per unit pore volume from induced polarization: A robust empirical relation fits multiple data sets. Geophysics 75:WA105–WA112. doi:10.1190/1.3471577

Wong, J. 1979. An electrochemical model of the induced-polarization phenomenon in disseminated sulfide ores. Geophysics 44:1245–1265. doi:10.1190/1.1441005

Zimmermann, E., A. Kemna, J. Berwix, W. Glaas, H.M. Münch, and J.A. Huisman. 2008. A high-accuracy impedance spectrometer for measuring sediments with low polarizability. Meas. Sci. Technol. 19:105603. doi:10.1088/0957-0233/19/10/105603